Phonon generation and decay in hydrogenated amorphous silicon

Marjolein van der Voort,[1] Andrey V. Akimov,[1,2] and Jaap I. Dijkhuis[1]
[1]*Faculty of Physics and Astronomy, Debye Institute, Utrecht University, P.O. Box 80.000, 3508 TA Utrecht, The Netherlands*
[2]*A.F. Ioffe Physical-Technical Institute, Russian Academy of Sciences, 194021 St. Petersburg, Russia*
(Received 28 January 2000)

We report on investigations of the temporal evolution of nonequilibrium phonon populations in hydrogenated amorphous silicon held at 1.8 K. Two types of *a*-Si:H were examined, one grown by plasma enhanced chemical vapor deposition (PE) and one by hot-wire assisted chemical vapor deposition (HW). Phonons were created during the relaxation and recombination of optically excited charge carriers, and detected by means of pulsed anti-Stokes Raman spectroscopy. In the same setup, pulsed luminescence experiments were performed, under identical experimental conditions. The temporal shape of the Raman signals turned out to be determined both by the electronic processes responsible for the phonon generation and by the anharmonic decay of the excited phonon population itself. In the PE films we observed a slowly decaying ($\gg 100$ ns) contribution to the Raman signal, which was not present in the HW layers. We propose a model to explain this slow background as resulting from laser-induced fast nonradiative recombination of mobile with localized charge carriers. The results of the pulsed luminescence experiments support our model. In addition, phonon decay times were observed to be the same in all samples: decay times of ~ 70 ns were obtained for LA- and TO-like vibrations, whereas TA-like vibrations decayed faster (<10 ns) than could be resolved with the experimental setup. We propose that the extreme longevity of the LA and TO phonons is related to the microstructure of amorphous silicon.

I. INTRODUCTION

An effective method to investigate dynamics of high-frequency phonons in amorphous semiconductors is provided by time-resolved Raman spectroscopy. Scholten *et al.*[1] employed this technique for the first time to examine transient phonon populations in (hydrogenated) amorphous Si held at 2 K, in a frequency range of 100 to 550 cm^{-1}. Especially interesting about this energy range is that it corresponds to the region where the exact nature of the vibrational excitations (for convenience called ''phonons'') in amorphous and glassy solids is still unclear. It is this frequency range, namely, where phonons are scattered to such a degree that the phonon mean free path approaches its wavelength.

The results of the early studies by Scholten *et al.* are still rather striking and under debate. First, the order of magnitude of the population decay times measured for phonons of the highest frequencies appeared to be about four orders of magnitude greater than for phonons of the same energies in crystalline Si (having a lifetime[2] of ~ 10 ps). Secondly, the dependence of the lifetime on phonon energy turned out to be opposite to what one generally observes in crystals: the measured decay times in *a*-Si *increase* with increasing energy. Identical results were obtained in *a*-Si and *a*-Si:H.

To explain these remarkable findings, it was proposed that in *a*-Si(:H) phonons with an energy higher than a critical value are strongly localized. It was suggested that a crossover (mobility edge) from extended to localized vibrations occurs at a phonon frequency well below the frequencies addressed in the experiments. In this explanation, the reduced decay rate is due to the fact that the localized excitations are decoupled from each other. A quantitative analysis of the data was presented in terms of the fracton model,[3] yielding good agreement between the measurements and the theoretical predictions, with a reasonable value for the anharmonic coupling constant.[4]

On the other hand, the outcome of computer simulations by Fabian and co-workers[5] disagrees with the above-mentioned experimental results and is at variance with the idea of localization as presumed in the fracton model. Anharmonic decay rates were calculated for vibrational states in a 216-atom model of *a*-Si. For these numerically built materials, it was found that the high-frequency modes decayed on picosecond time scales, and at low temperatures vibrational lifetimes *decreased* with increasing frequency, as in crystals. Further, a mobility edge and crossover from extended to localized modes were detected. However, the crossover frequency was determined to exceed the highest frequencies studied by Scholten *et al.* Moreover, even the localized modes have picosecond lifetimes according to these calculations.

One important difference between the calculations and the experiments lies in the influence of the electronic properties of the amorphous semiconductor on the vibrational dynamics. In the experiments, vibrations are generated during the relaxation of optically excited charge carriers. At low temperatures, the electronic excitations may persist for milliseconds,[6] which complicates the interpretation of the observed vibrational signals. In the computer models of *a*-Si, electronic processes are not considered at all. Another point is that, both in the fracton model and in the computer simulations, *a*-Si is assumed to be statistically homogeneous, which, as some authors claim, is not realistic.[7] As a consequence, in both approaches the possibility is ignored that structural inhomogeneities, like voids, affect the vibrational dynamics in *a*-Si(:H).

In this paper, we present results of pulsed anti-Stokes Raman and luminescence experiments on two types of *a*-Si:H.

One type of layer was grown by ''conventional'' plasma enhanced (PE) chemical vapor deposition, and the second by the relatively new hot-wire (HW) assisted chemical vapor deposition method. With the latter growing technique, more stable amorphous structures can be produced.[8] In the present study we were further able to monitor the temporal evolution of a vibrational population during a much longer period after its creation and over a larger frequency range than was possible previously with the setup used by Scholten *et al*. This fact, and the combination of anti-Stokes Raman and luminescence experiments performed under the same experimental conditions, allowed us to investigate the influence of electronic processes on the vibrational signals. Indeed, the interplay of electronic and vibrational processes in *a*-Si:H has received much attention recently,[9] because of its suspected role in the light-induced degradation of this material, also known as the Staebler-Wronski effect.[10,11] Further, the results of our experiments confirm the longevity of phonons in *a*-Si:H reported by Scholten *et al*. Finally, we discuss the possibility that the long lifetimes are related to the microstructure of the amorphous silicon material.

II. EXPERIMENTAL DETAILS

A. Samples

Device-quality intrinsic *a*-Si:H layers were prepared in two different ways. The first type of sample (PE) was grown by means of plasma enhanced chemical vapor deposition in a system described by Madan *et al.*[12] One micrometer of *a*-Si:H material was deposited on a crystalline silicon wafer held at a temperature of 320 °C. The layers contained about 11 at. % hydrogen. Other samples (HW) with thicknesses of 1.0 and 1.5 μm were prepared by hot-wire assisted chemical vapor deposition,[13] again on *c*-Si substrates, held at 450 °C. The hydrogen concentration of the HW material amounted to 8 at. %. The thickness of the *a*-Si:H samples was chosen to be much larger than the penetration depth ($\sim$100 nm) of the green light used in the measurements.

Room-temperature Stokes Raman spectra of the two types of *a*-Si:H layers show that the TO peak centered at 480 cm^{-1} has a slightly narrower width in the case of the HW material than for the PE layers (half width at half maximum of 32 ± 0.5 cm^{-1} compared to 34 ± 0.5 cm^{-1}). These numbers suggest that the material of the HW samples is slightly less disordered than that of the PE layers,[14] which makes a comparison of the observed vibrational dynamics in the two types of *a*-Si:H of particular interest.

Feenstra *et al.* examined the optoelectronic material properties of *a*-Si:H layers deposited on glass substrates, in the same apparatus and under the same deposition conditions as for the samples we used.[15] Their investigations indicate that the (Tauc) band gaps of our samples are 1.7 and 1.78 eV for the HW and PE layers, respectively. These numbers will be used in the quantitative analysis of the experimental results. For the concentration of defect states, they found densities of 3×10^{16} cm^{-3} and 5×10^{15} cm^{-3} for as-grown HW and PE samples, respectively. Under illumination, these numbers increased to 2×10^{17} cm^{-3} in the case of HW *a*-Si:H and 1×10^{17} cm^{-3} for the PE film. The concentration of tail states in both types of material is of the order of 10^{20} cm^{-3}.

B. Pulsed Raman and luminescence experiments

The samples were immersed in superfluid He ($T = 1.8$ K) to remove the thermal population of vibrations in the energy range of interest. Then a vibrational population was created by means of optical excitation. Absorption of green photons with an energy ($\sim$2.3 eV) larger than the gap results in the excitation of charge carriers. These hot carriers relax on a picosecond time scale[16] to localized states in the band tails, converting their excess energy into phonons. The relaxation process proceeds via recombination, in which radiative and nonradiative decay channels compete, the latter being an additional source of vibrational excitations.

In the experiments described below, phonons were generated by the output of two frequency-doubled, *Q*-switched Nd:YAG (yttrium aluminum garnet) lasers (2.33-eV photons, with a penetration depth in *a*-Si:H of $\sim$100 nm). Both lasers produced pulses with a width of $\sim$10 ns (full width at half maximum) at a rate of 30 Hz. The beams were made collinear and focused to a ~ 1 mm^2 spot on the sample, where the average excitation power per beam typically amounted to 5 mW. By means of polarization rotators, the specular reflections of both beams from the sample were minimized, thereby maximizing the amount of light absorbed. The resulting absorbed energy density per pulse amounted to $\sim 1.5 \times 10^3$ J/cm^3.

Scattered light was collected in a backscattering geometry and projected onto the entrance slit of a triple-grating monochromator equipped with a liquid-nitrogen-cooled charge-coupled device (CCD) detector. Anti-Stokes Raman spectra were recorded with a 15-min exposure time of the CCD camera. The spectral resolution was ~ 40 cm^{-1}.

To investigate the temporal evolution of the phonon population created, pulses of one of the lasers (''probe'') were electronically delayed with respect to those of the other (''pump''). Then, by measuring anti-Stokes intensities as a function of the delay Δt between the pump and probe pulses, the dynamics of nonequilibrium phonons was examined in the range of 10 ns up to 15 ms.

Apart from Raman scattering, luminescence produced by the radiative recombination of excited carriers could also be detected. Because radiative and nonradiative recombination processes are competing in the relaxation path described above, luminescence experiments also provide useful information about nonradiative recombination and phonon generation, as we will show.

Pulsed luminescence measurements were performed with the same pump-probe configuration as used for the pulsed Raman experiments, under identical experimental conditions. Only the spectral window selected by the triple-grating monochromator was shifted. Limited by the range of the gratings, a window of 1.53–1.45 eV was chosen. In *a*-Si:H, luminescence at these energies is caused by radiative recombination of electrons and holes trapped in the tail states. In the case of the luminescence measurements, spectra were recorded with a 2.5-min exposure time of the detector.

III. RESULTS

A. Pump-probe anti-Stokes Raman spectroscopy

In Fig. 1 time-integrated anti-Stokes Raman spectra of both the PE and HW samples are presented, in each case for

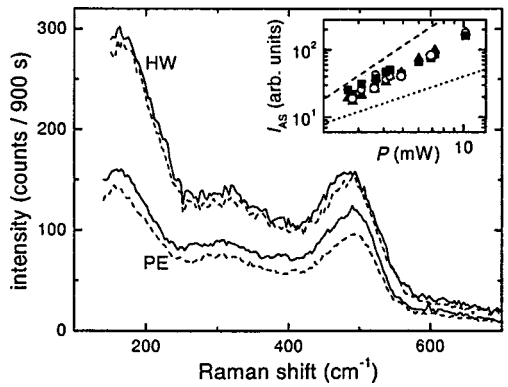

FIG. 1. Anti-Stokes Raman spectra of the HW and PE samples (upper two curves and lower two curves, respectively), measured at 1.8 K, for $\Delta t = 100$ ns (solid lines) and $\Delta t = 15$ ms (dashed lines). The inset shows the dependence of the (normalized) anti-Stokes Raman intensity I_{AS} on excitation power, measured in HW-grown *a*-Si:H, for excitation with one laser beam (■ = TO, ▲ = LA, and ○ = TA). The dotted and dashed lines indicate linear and quadratic dependences, respectively.

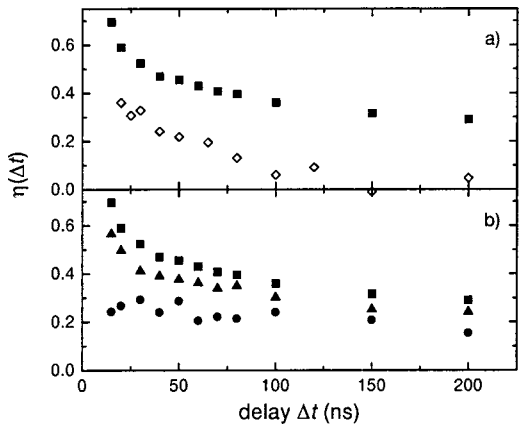

FIG. 2. (a) Normalized time-dependent anti-Stokes signal $\eta(\Delta t)$ of the TO phonons as a function of Δt in the HW (◇) and PE (■) samples. (b) $\eta(\Delta t)$ vs Δt measured in PE *a*-Si:H (■ = TO, ▲ = LA and ● = TA).

delays Δt of 100 ns and 15 ms. All spectra exhibit the characteristic bands centered at 150, 300, and 480 cm^{-1}, corresponding to TA-, LA-, and TO-like vibrations in *a*-Si(:H).[17]

Since the spectrometer settings were not identical in the experiments on the two samples, the relative intensities of different peaks in the upper and lower two curves of Fig. 1 cannot be directly compared. The suppression of elastically scattered light was lower in the case of the measurements on the HW layer, resulting in the relatively high intensity in the spectral region of the TA phonons. However, the difference in the overall intensities of the signals of the two types of *a*-Si:H is real. Accurate measurements of the anti-Stokes spectra of the two layers, under exactly the same experimental conditions, namely, confirmed that the signal intensities in the HW sample are higher. In the case of excitation with one laser beam (power ~3 mW), the height of the anti-Stokes spectrum of this sample at all frequencies exceeds that of the PE layer by a factor of ~1.4, even though the absorbed energy density in the two types of *a*-Si:H is virtually the same.

For both samples, the dependence of the Raman intensity on excitation power was studied in the case of excitation with one laser beam. The Stokes signals I_ω^S are observed to increase linearly with P, whereas the anti-Stokes signals I_ω^{AS} exhibit for all frequencies an almost quadratic dependence on P. The inset of Fig. 1 illustrates the P^2 dependence of the anti-Stokes intensity measured for HW *a*-Si:H. These results are consistent with the results reported earlier by Scholten *et al.* for PE-grown *a*-Si:H and *a*-Si.[1] From the ratio between I_ω^S and I_ω^{AS}, the phonon occupation numbers n_ω can be computed, with the help of the relation $n_\omega = I_\omega^{AS}/(I_\omega^S - I_\omega^{AS})$. For the range of frequencies and powers addressed in the experiments, n_ω ranged between ~0.03 and 0.3, so that $n_\omega \approx I_\omega^{AS}/I_\omega^S$. Then, the observations that $I_\omega^S \propto P$ and $I_\omega^{AS} \propto P^2$ indicate that n_ω increases linearly with P, independent of ω. The conclusion that the shape of the phonon spectrum excited does not change with P demonstrates that the phonon distribution studied is not thermalized but has a nonequilibrium character.[1]

A remarkable feature of Fig. 1 is that, in the PE sample, the anti-Stokes intensity $I_\omega^{AS}(\Delta t)$ significantly drops on going from $\Delta t = 100$ ns to 15 ms, whereas $I_\omega^{AS}(\Delta t)$ remains constant in the HW layer. To examine this point in more detail, a series of anti-Stokes spectra was recorded as a function of Δt. The time-dependent contributions to the signals were obtained by subtracting a background spectrum taken with $\Delta t = 15$ ms from each measurement. $I_\omega^{AS}(\Delta t)$ measured for $\Delta t = 15$ ms, namely, was equal to the sum of the separate contributions of the two lasers. In Fig. 2(a), the normalized time-dependent anti-Stokes intensity $\eta(\Delta t) = [I_\omega^{AS}(\Delta t) - I_\omega^{AS}(15\text{ ms})]/I_\omega^{AS}(15\text{ ms})$ of both types of *a*-Si:H is plotted vs the delay Δt, for the TO part of the spectrum. Figure 2(b) shows the contributions from different parts of the phonon spectrum of the PE sample only. To improve signal-to-noise ratios, all intensities were integrated over a range of frequencies: 140–220 cm^{-1}, 240–380 cm^{-1}, and 420–550 cm^{-1} for the TA, LA, and TO modes, respectively. Within the selected spectral regions, no dependence of the decay rate on frequency could be observed. In both types of film, a relatively fast decay time $\tau \sim 70$ ns is measured for the TO spectral region. However, in the PE sample, $I_\omega^{AS}(\Delta t)$ does not decay to zero, but instead to a slowly ($\gg 100$ ns) decaying background. The level of this background depends on excitation power. For excitation with half of the power of both laser beams, the absolute value of the background $I_\omega^{AS}(\Delta t \sim 200\text{ ns}) - I_\omega^{AS}(15\text{ ms})$ is about half of the value observed with full power (5 mW). In the frequency region of the TO phonons, this corresponds to an $\eta(\Delta t \sim 200\text{ ns})$ of ~30%, in the case of excitation with full power. The slow contribution is observed in the PE sample for the TO as well as the LA and TA modes, but seems absent in the HW sample. Yet, in measurements of the transient anti-Stokes spectra of PE *a*-Si:H grown in a different laboratory,[18] it showed up again, suggesting that it is characteristic for PE-grown *a*-Si:H.

Next, the time-dependent part of the signals will be considered. According to Fig. 2(b), in the LA region of the spectrum the population decays on about the same time scale as the TO part. The decays are nonexponential, and can be characterized by a mean decay time $\langle \tau \rangle$, of 70 ± 10 ns. Here, we used the relation $\langle \tau \rangle = \int t I_\omega^{AS}(t)dt / \int I_\omega^{AS}(t)dt$, with I_ω^{AS} cor-

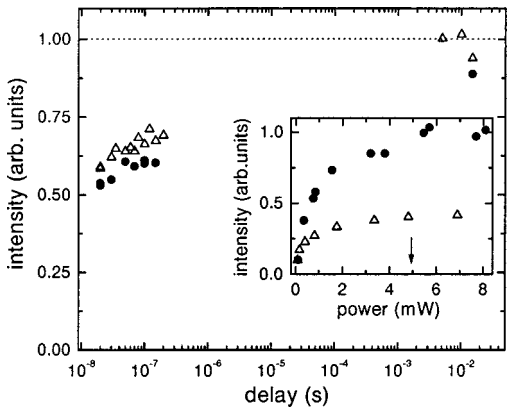

FIG. 3. Luminescence intensity at 840 nm of HW (△) and PE (●) *a*-Si:H as a function of Δt, normalized to the sum of the luminescence intensities obtained with each laser separately (dotted line). The measurements were performed under identical experimental conditions as the Raman experiments. The inset shows the dependence of the luminescence intensities excited with a single laser beam on excitation power, again for HW (△) and PE (●) *a*-Si:H. The arrow indicates the typical power used for the time-resolved Raman and luminescence experiments.

rected for the background. Decay times of the TA part of the spectrum are too short to determine with the experimental setup. With the exception of the slow background, the spectra of the HW sample exhibit the same behavior (not shown). In both samples, the value of the decay times obtained appeared not to depend on excitation power.

Similar experiments on a bare *c*-Si substrate did not show any transient anti-Stokes contributions, confirming that the results presented above reflect the generation and decay of phonons in the *a*-Si:H layers.

B. Pump-probe luminescence measurements

Luminescence experiments were performed under the same experimental conditions as the Raman measurements. The inset of Fig. 3 shows how the intensity of the tail state luminescence of the two types of *a*-Si:H layer depends on excitation power, in the case of excitation with one laser beam. Obviously, the luminescence is saturated for the typical excitation powers (5 mW) used in the time-resolved Raman experiments. For these large absorbed energy densities, nonradiative (so called ''bimolecular'') recombination dominates the final recombination step in the relaxation of the excited charge carriers.[19] We note that the saturation level reached for the PE sample is two times higher than the maximum luminescence intensity produced by the HW sample (note that the anti-Stokes signals were higher in the HW layer). This suggests a difference in the ratios of radiative and nonradiative recombination rates in the two types of *a*-Si:H. Indeed, if nonradiative recombination is slower in PE-grown a-Si:H, both the higher saturation level of the luminescence and the lower anti-Stokes Raman signals in this material can be explained, as will be shown later.

In Fig. 3, results of the pump-probe luminescence measurements are presented. The luminescence intensities are normalized to the sum of the luminescence intensities obtained with the pump and probe separately. For delays of several milliseconds, the luminescence generated in the HW layer equals this sum. For the excitation powers (5 mW) that were used for the Raman measurements, it was not possible to record spectra for Δt's between ~ 1 μs and 1 ms, due to the appearance of a helium bubble caused by the vaporization of liquid He at the sample surface. For excitation powers one order of magnitude lower, the luminescence could be monitored over the full range of delay times. The intensity appeared to increase gradually with the delay, until a maximum was reached after ~ 10 ms. The characteristic time scale of the luminescence is comparable with the slowly decaying background observed in the Raman signals, which suggests that the latter is related to electronic processes.

Finally, we note that no fast contributions to the time-dependent signals are observed.

TABLE I. Main characteristics of the two contributions to the anti-Stokes Raman signals. It should be noted that the $q<2$ power dependence of the slow component was not investigated in detail.

		Fast component	Slow component
Sample type	PE	present	present
	HW	present	absent
Decay time at	TA	<10 ns	~ 1 ms
	LA	~ 70 ns	~ 1 ms
	TO	~ 70 ns	~ 1 ms
Power dependence	$I_{AS} \propto P^q$	$q \sim 2$	$q<2$

IV. DISCUSSION

Two contributions to the transient anti-Stokes Raman signals were observed (see Fig. 2): a relatively fast decaying part, and a slow background. Their main characteristics are summarized in Table I. Obviously, the two components behave quite differently. Both, however, are related to nonequilibrium vibrational populations. To demonstrate this, we resort to the same arguments as presented by Scholten *et al.*, which are based on the observed excitation power dependence of the Raman spectra and the frequency dependence of the obtained decay times.[1] From the quadratic increase of the anti-Stokes Raman intensity with excitation power, and the linear dependence of the Stokes intensity on P, one can conclude that the shape of the phonon spectrum excited is independent of P. In contrast, in the case of thermal equilibrium, the phonon occupation would be described by the Bose-Einstein distribution, characterized by an equilibrium temperature increasing with P. Consequently, the shape of the spectrum would significantly depend on P, which is not observed. Further, the decay rate of a phonon population obeying Bose-Einstein statistics is an increasing function of ω.[1] However, both the ''slow'' and ''fast'' contributions to the Raman signals exhibit no indications of an increase of $\langle \tau \rangle^{-1}$ with ω.

These two arguments lead us to the conclusion that a nonequilibrium phonon distribution was present in our experiments, in the PE as well as in the HW *a*-Si:H layers. Both the fast and slow components in the signals originate from this nonequilibrium population.

A. Electronic and vibrational contributions

Now that we know that the phonon population monitored via the anti-Stokes Raman intensity has a nonequilibrium character, the next question is what causes its decay. Since all decay times obtained are several orders of magnitude longer than the anharmonic decay times of phonons generally observed in crystals, it is difficult to believe that these times correspond to the bare lifetimes of phonons in amorphous silicon. Actually, it has been suggested that, due to disorder, the effect of anharmonicity in *a*-Si is even larger than in *c*-Si, which would result in an increased anharmonic decay rate in *a*-Si, instead of a slower decay.[5]

An explanation one could think of is not that the phonons have long lifetimes, but that the source of electronic excitations that generate the phonons is long lived. The vibrational signals may persist much longer than the phonons exist if the absorbed energy is not transformed instantaneously into phonons, but is accumulated in the electronic system of the amorphous semiconductor. Indeed, carriers that are trapped in the tail states of *a*-Si:H are known to have up to millisecond lifetimes at low temperatures[6] (see also Fig. 3). However, the very occurrence of electronic processes that have characteristic time scales comparable with the decay times of the Raman signals does not necessarily explain our experimental results. Of course, the amount of phonons created in the electronic processes should also agree with the observed phonon occupation numbers. Some rough estimates are given now to illustrate that only phonon generation and decay rates in a certain range can account for the measured occupation numbers.

Occupation numbers and lifetimes: Some estimates

In the excited *a*-Si:H volume, roughly 0.75×10^{16} optical phonon modes are available. We assume for simplicity that all these modes have a frequency that corresponds to the TO part of the Raman spectrum. Then, the maximum number of quanta that can be created from the ~150 μJ energy absorbed during a pulse is $\sim1.6\times10^{16}$. If the phonons in the excitation volume are generated at a constant rate G during the laser pulse, and the population decays exponentially with a time constant τ, the occupation n of the modes in the excited volume at time t during the pulse can be written as $n(t)\approx G\tau[1-\exp(-t/\tau)]/(0.75\times10^{16})$.

In the case that the population decay time τ is much shorter than the duration of the laser pulse and assuming that all electronic energy is converted to phonons during the laser pulse, we arrive for $n=0.15\pm0.05$ at a minimal average population decay time of 700 ps under the relevant excitation conditions, which is much longer than the crystalline TO lifetime. Even when the majority of the modes has a picosecond population lifetime as expected from computer simulations[5] and consequently does not contribute to the anti-Stokes Raman signal, the remaining part must reach a correspondingly higher n and have a longer τ in order to explain the measurements. If we associate the measured 70 ns time with the phonon population decay, then the average population number of the long-lived modes reached during the laser pulse is $n(5\text{ ns})=1.0$. Then, 15% of the phonon modes would have a long lifetime and 85% a short lifetime. If we alternatively assign the 70 ns lifetime to decay of the phonon source, we are still facing the minimal 700 ps average lifetime calculated above. In all cases, the measured decay of the anti-Stokes Raman signals inevitably leads to the conclusion that at least some of the phonon modes in hydrogenated amorphous silicon have a population decay time that exceeds the expected anharmonic TO lifetime by orders of magnitude.

From these considerations it also follows that we can account for the high phonon occupation numbers observed only if a large number of phonons is created during a short period. A scenario that may satisfy this constraint is that part of the energy absorbed is stored in the form of long-lived electronic excitations, for instance, by means of a tail state population. If this stored energy can be released quickly by renewed optical excitation, relatively high phonon populations could be generated with a second laser pulse.

In that case, the spectral distribution of the ''extra'' phonons that are created with the second pulse is not expected to depend on the delay between the pump and probe pulses, since the energy distribution of the electronic excitations remains unaltered in the period between two laser pulses. We note that the shape of the Raman spectra measured for long delay times ($\Delta t>100$ ns) weakly depends on Δt, in contrast to the behavior on short time scales. For a delay larger than the laser pulse width (10 ns) we completely lose the TA contribution around 150 cm^{-1} apart from the slowly decaying background, but at the same time keep the extra LA and TO signals on top of the background, which is incompatible with electronic effects. This suggests that the slow part of the anti-Stokes Raman signals indeed is of electronic origin, while the fast part is related to phonon population decay.

In the next two subsections, both the electronic and vibrational contributions to the temporal shape of the anti-Stokes Raman signals will be discussed in more detail.

B. Electronic contribution to the vibrational signals

Since the slow ($\gg100$ ns) contribution to the anti-Stokes Raman signals cannot be accounted for by just the longevity of the phonons ($\tau<100$ ns), we reconsider the mechanisms of phonon generation. We take the point of view that part of the phonon generation occurs during the first laser pulse, synchronously with the absorption of the green photons, whereas another part is triggered by the absorption of the second laser pulse.

Phonons are produced at various stages in the process of carrier relaxation that follows the photoexcitation of *a*-Si:H. The first step, thermalization, takes place on a picosecond time scale.[16] Hence it is too fast to explain the slow background. However, the second stage, recombination, may be slow if carriers localized in the tail states are involved. In the absence of optical pumping, the lifetime of carriers in the tail states is known to be as long as ~1 ms,[6] i.e., of the right order to match the slow contribution to the Raman signals. The recombination of electrons and holes that are both trapped in the tail states is far too slow to account for the measured occupation numbers. But the recombination of free carriers with carriers trapped in the tail states is efficient enough to play an essential role in the phonon generation, as will be demonstrated below.

The idea is roughly as follows. During the first laser pulse, phonons are created both due to relaxation of carriers to the band edges, and due to nonradiative recombination. Of course, all phonons contribute to the Raman signal. At the same time, tail states are filled with electrons and holes, and energy is stored. Because of the long lifetimes of these states, trapped carriers survive the period between the first and second laser pulses (for delays up to ~ 1 ms). Consequently, at the start of the second laser pulse, many tail states are still occupied. The abundantly present free carriers freshly created by the probe quite efficiently recombine with the trapped ones. As a result, the number of nonradiative transitions, and hence the phonon generation rate during the second laser pulse, is higher than during the first pulse. In other words, even if the total phonon population has vanished, the second pulse may induce a more intense anti-Stokes Raman spectrum than the first.

1. Model: Importance of the relative rates of relaxation and recombination

To investigate the idea more quantitatively, we resort to a simple rate-equation model that connects the concentrations of free carriers (N_f), trapped carriers (N_t), and phonons of frequency ω (N_ω). For simplicity, both the thermalization rate of free carriers, w, and the bimolecular recombination rate C are taken equal for electrons and holes. Further, radiative decay is not taken into account, consistent with the fact that nonradiative processes dominate the recombination for the excitation powers used in the experiments. Also, recombination of trapped holes with trapped electrons is neglected, because of the intrinsically low rates of such processes. Thus, we arrive at the following coupled rate equations for the carrier concentrations:

$$\dot{N}_f = g(t) - wN_f - CN_f(N_f + N_t) \quad \text{and}$$

$$\dot{N}_t = wN_f - CN_fN_t. \tag{1}$$

The term $g(t)$ describes the generation of free carriers by pulsed optical excitation and is determined by P, and is taken constant during the pulse. The term wN_f relates to the trapping of free carriers at the tail states. The phonon generation rate due to relaxation is proportional to this component. The contributions involving C correspond to the nonradiative recombination of free carriers with free and trapped carriers, where $CN_f(N_f+N_t)$ describes the phonon generation rate caused by recombination, and the rate constants are taken equal. Because relaxation to the band edges is much faster than the other processes, this term is approximated by CN_fN_t.

The total phonon generation rate $G_{ph}(t)$ is equal to the sum of the contributions originating from relaxation and recombination. The ratio of the amount of energy released by relaxation to the amount of energy released during recombination, β, is determined by the difference in energy between the photons that excite the carriers, E_{YAG}, and the gap, E_{gap}, of a-Si:H, so that $\beta=(E_{\mathrm{YAG}}-E_{\mathrm{gap}})/E_{\mathrm{gap}}$. Thus, the generation rate for phonons of frequency ω is described by

$$G_{ph}(t) \propto CN_fN_t + \beta wN_f. \tag{2}$$

If we assume, for simplicity, that phonons decay monoexponentially with a decay time τ_ω that depends only on the phonon frequency, the concentration of phonons of that frequency is given by

$$\frac{dN_\omega(t)}{dt} = G_{ph}(t) - \frac{N_\omega(t)}{\tau_\omega}. \tag{3}$$

Then, if the sample is excited with a laser pulse of length t_1, starting at $t=0$ and causing an average carrier generation rate g, the anti-Stokes Raman intensity for phonons of frequency ω due to this pulse is $I_\omega^{\mathrm{AS}} \propto g\int_0^{t_1} N_\omega(t)dt$, where $N_\omega(t)$ is obtained from solving Eqs. (1) and (3).

Our goal is to investigate if the presence of electronic excitations may increase the height of the anti-Stokes Raman spectrum detected with a second laser pulse as compared to the spectrum detected with the first pulse only, even in the case that the nonequilibrium phonon population has completely decayed between the pulses. Therefore, the situation is considered where a second laser pulse, of the same width and intensity as the first pulse, succeeds the first pulse after a period Δt much longer than the phonon decay time τ_ω. At the same time, Δt is taken much shorter than the lifetime of the tail states, so that at the start of the second pulse, N_t has the same value as at the end of the first. In practice, that would correspond to a Δt between 10 ns and 0.1 ms for phonons with the shortest lifetimes (TA) and to a Δt between ~ 200 ns and 0.1 ms for the long-lived TO phonons. From the pump-probe luminescence measurements shown in Fig. 3 we know that indeed, in both samples studied, electronic excitations survive the delays that are relevant for the Raman experiments.

To simplify the calculations, two extreme cases are distinguished. In the first case we consider, the phonon decay time is much shorter than the duration of the laser pulse ($\tau_\omega \ll t_1$), as is the case for TA phonons. Then, we may assume that the population decay is in equilibrium with the phonon generation, so that $\dot{N}_\omega \approx 0$ and $N_\omega(t) = G_{ph}(t)\tau_\omega$. Consequently, the anti-Stokes Raman intensities detected with the first and second laser pulses, $I_{\mathrm{TA}}^{(1)}$ and $I_{\mathrm{TA}}^{(2)}$, respectively, are proportional to

$$I_{\mathrm{TA}}^{(i)} \propto g\tau_\omega \int_0^{t_1} G_{ph}^{(i)}(t)\,dt, \tag{4}$$

with $i=1,2$. The second situation occurs when the phonon decay time is much longer than the pulse duration ($\tau_\omega \gg t_1$), but still much shorter than Δt. This is the case for TO phonons. Under these circumstances, the phonon population increases as long as phonons are generated, and $\dot{N}_\omega \approx G_{ph}$ and $N_\omega(t) = \int_0^t G_{ph}(t')dt'$. This leads to anti-Stokes Raman intensities $I_{\mathrm{TO}}^{(i)}$ described by

$$I_{\mathrm{TO}}^{(i)} \propto g \int_0^{t_1} \int_0^t G_{ph}^{(i)}(t')\,dt'\,dt. \tag{5}$$

Exact solutions of Eq. (1) can be obtained and used to evaluate the integrals of Eqs. (4) and (5). In this way, the curves presented below were obtained. Note that the calculated sum $I_{\mathrm{TO}}^{(1)} + I_{\mathrm{TO}}^{(2)}$ can be identified with the experimentally obtained intensity $I_{\mathrm{TO}}^{\mathrm{AS}}(\Delta t)$ for a Δt between ~ 200 ns and ~ 0.1 ms.

Correspondingly, we define $\eta_{\mathrm{calc}}=(I_{\mathrm{TO}}^{(2)}-I_{\mathrm{TO}}^{(1)})/2I_{\mathrm{TO}}^{(1)}$, analogous to the experimental $\eta(\Delta t)$.

2. Application to the experiment

To apply the model to the experiments, numerical values have to be substituted for the parameters. Of these parameters, β, C, and w depend on the type of material. As already mentioned, the Tauc gap of the *a*-Si:H layers used is 1.7 eV for the HW sample and 1.78 eV for the PE layer, corresponding to $\beta=0.37$ and $\beta=0.31$, respectively. Values for C and w are at present not available for exactly these two samples and are therefore taken from the literature. Values given for C vary between 2×10^{-9} $\mathrm{cm^3\,s^{-1}}$ and 2.3×10^{-8} $\mathrm{cm^3\,s^{-1}}$.[9,20–22] For the thermalization rate w, values between 10^{13} $\mathrm{s^{-1}}$ and 10^{12} $\mathrm{s^{-1}}$ have been found.[21] In the calculations, only the ratio of C/w enters the equations. From the numbers given here, we find that the values for C/w range from 2×10^{-22} $\mathrm{cm^3}$ to 2.3×10^{-20} $\mathrm{cm^3}$. Finally, g is estimated from the pulse energy and pulse width, assuming that all absorbed photons produce an excited electron.

Now the contributions of carrier recombination and relaxation to the TO anti-Stokes Raman intensities can be calculated, for different combinations of C/w and β. Exploratory calculations were performed for two values of C/w, 5×10^{-22} $\mathrm{cm^3}$ and 5×10^{-21} $\mathrm{cm^3}$, and $\beta=0.31$ taken the same in both cases. From that calculation, we learned that only for the lower of the two values taken for C/w, 5×10^{-22} $\mathrm{cm^3}$, the total intensity measured with the second pulse was higher than that measured with the first pulse. Since that result was closest to the situation we encountered for the PE sample, and the curves for the other value of C/w appeared to agree with the experimental results obtained for HW *a*-Si:H, the calculation was repeated. During the second evaluation, the Raman intensities were calculated for combinations of the lower C/w with $\beta=0.31$ corresponding to the PE sample, and the higher C/w with $\beta=0.37$ of the HW layer. The results of that calculation are presented in Figs. 4 and 5. We note that differences in the results for the two combinations of C/w and β hardly depend on β.

From Fig. 4, it can be seen that it is indeed possible to obtain an ''extra'' contribution to the anti-Stokes Raman signals measured with a second pulse, as compared to the intensities obtained with a first pulse, even in the case that *all phonons have decayed* during the delay time between these two pulses. The combination of the values for the excitation power and material parameters determines if this extra contribution is present or not. This explains why a ''background'' signal was observed in the PE sample, and not in the HW *a*-Si:H layer. These graphs further show that both relaxation and nonradiative recombination contribute significantly to all signals obtained.

In Fig. 5(a) the ratio of the total TO intensity measured with the first pulse, as predicted for the two combinations of C/w and β, is plotted as a function of P. According to the calculation, the total intensity should be between 1.2 and 1.6 times higher for the case that $C/w=5\times10^{-21}$ $\mathrm{cm^3}$ and $\beta=0.37$ (the HW case) than for the other combination (the PE case). This is consistent with the result that, for an excitation power of 3 mW, the anti-Stokes signal obtained in the HW sample was 1.4 times higher than that measured in the PE

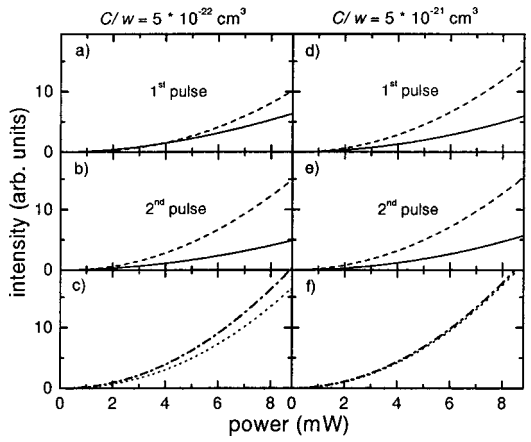

FIG. 4. Calculated TO anti-Stokes Raman intensities vs P for $C/w=5\times10^{-22}$ $\mathrm{cm^3}$ and $\beta=0.31$ [(a), (b), and (c)] and $C/w=5\times10^{-21}$ $\mathrm{cm^3}$ and $\beta=0.37$ [(d), (e), and (f)]. For both combinations of C/w and β, the contributions to the signals due to relaxation (solid lines) and nonradiative recombination (dashed lines) are given, that are produced by the first laser pulses [(a) and (d)] and the second laser pulse [(b) and (e)]. The curves in (c) and (f) display the total anti-Stokes Raman intensities calculated for the first and second laser pulse ($I_{\mathrm{TO}}^{(1)}$ and $I_{\mathrm{TO}}^{(2)}$, dotted and dash-dotted lines, respectively).

film. It is important to mention in this context that the difference in signal intensities measured in the PE and HW samples is not caused by a difference in absorption. The difference is exclusively due to the different values of the ratio C/w.

According to the model, the number of phonons produced during the laser pulses in the PE sample is lower than in the HW layer, which is consistent with the observation that the luminescence intensity in the PE film exceeds that of the HW sample (see inset of Fig. 3). If the nonradiative recombination rate C is lower in PE *a*-Si:H, indeed a higher saturation level of the luminescence is expected for the PE sample. If, in addition, w is of the same order in both materials, C/w is lower for the PE sample, as is also suggested by the outcome of the above calculations.

To further compare the model with the experiments, we show in Fig. 5(b) the calculated η_{calc} as a function of exci-

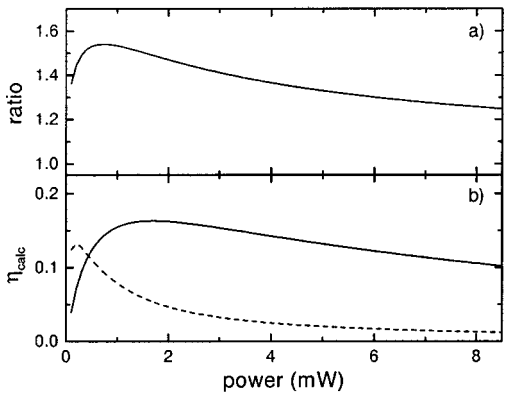

FIG. 5. (a) Calculated total intensity measured with the first pulse for $C/w=5\times10^{-21}$ $\mathrm{cm^3}$ and $\beta=0.37$ (HW case), divided by the total intensity obtained with the first pulse for $C/w=5\times10^{-22}$ $\mathrm{cm^3}$ and $\beta=0.31$ (PE case), as a function of P. (b) η_{calc} vs P, for the PE and HW case, solid and dashed lines, respectively.

tation power for both combinations of C/w and β. For the typical excitation power used during the Raman measurements (5 mW), η_{calc} amounts to $\sim 13\%$ for the PE case and $\sim 2\%$ for the HW case, in qualitative agreement with the experimental observations.

We note that the curves presented in Figs. 4 and 5 have been calculated in the long-phonon-lifetime limit (TO phonons), but that results obtained for the TA phonons are qualitatively the same. In other words, the slow contribution to the signals behaves similarly for different phonon frequencies, as was observed experimentally.

The analysis leading to Eq. (1) allows us to estimate the densities of free and localized carriers for our experimental conditions. For the HW sample we arrive at values of 5×10^{20} cm^{-3} and 1×10^{16} cm^{-3} for the trapped and free carriers, respectively, and for PE at 2×10^{20} cm^{-3} and 1×10^{16} cm^{-3}, respectively, in both cases for the maximum excitation power used in the experiments. The value for localized carriers is of the same order of magnitude as or even slightly higher than the density of the available tail states[15] ($\sim 10^{20}$ cm^{-3}). For reasons of tractability, our simplified model takes into account only two classes of carriers, localized and free ones. In reality there are also intermediate cases of carriers that undergo down-hopping between tail states. One may argue that these processes could well occur on a nanosecond time scale and thus be responsible for the experimentally observed 70 ns decay. This view, however, is incompatible with the much faster decay time observed for TA phonons, whereas the slowly decaying background is detected for all phonon energies (Fig. 2).

In our analysis, we assume that all absorbed energy is either present in the form of electronic excitations or directly released by emission of phonons, which may in fact not be the case. Branz, for example, stated that, during the relaxation of photoexcited carriers in *a*-Si:H, SiH bonds may break,[11] leading to dangling bonds and mobile hydrogen atoms. The mobile H diffuses through the material, and is either retrapped at a dangling bond at another location, or forms, together with another excited mobile H atom, a metastable H_2 complex. In both cases, energy is temporarily stored in a ''cloud'' of mobile H atoms, which prevents the generation of phonons. This would mean that we overestimate in the above model both the number of phonons created during thermalization and the population formed during recombination of the excited carriers. To explain the background, however, primarily the ratio of the amounts of phonons produced during the two processes is of importance. If energy is taken up and stored by alternative kinds of excitations, for instance, mobile H atoms, the background may be accounted for with lower occupation numbers of the electronic populations. So the main point we make with the model is that a significant part of the total energy that is eventually converted into phonons is released only when the sample is excited with a second pulse, as long as that pulse appears within the electronic lifetime of the tail states. In this way, the presented model qualitatively explains why a slow background contribution to the transient anti-Stokes Raman signals was observed, without the need to invoke extreme longevity ($\tau \gg 100$ ns) of phononlike modes in *a*-Si:H.

C. Phonon decay in amorphous silicon

As discussed above, we interpret the fast contributions to the Raman signals as corresponding to the lifetimes of ''phonons'' in *a*-Si:H. Hence, the results of our experiments indicate that high-frequency vibrations in *a*-Si:H can have lifetimes up to ~ 70 ns, i.e., several orders of magnitude longer than in crystals. This observation is in quantitative agreement with the results of the Raman measurements reported by Scholten *et al.* Also, in different types of experiment, indications for the existence of such long-lived phonons in amorphous solids have been found.[23–25]

Theoretical descriptions that are consistent with the occurrence of lifetimes of the order of magnitude observed in the experiments are the fracton model[3] and the hopping model by Damker *et al.*[27] Both models involve the localization of the major part of the vibrational modes in *a*-Si and the assumption that the anharmonic decay of localized into localized vibrations can be neglected. In contrast, numerical simulations based on the diffuson model predict that most of the vibrational excitations in *a*-Si are extended.[5] According to these simulations, and to the results of more recent molecular dynamics calculations,[28] vibrations of the frequencies addressed in our experiments are extended (diffusions) and have picosecond lifetimes.

A difficulty that arises when comparing the theoretical descriptions with the experiments is that it is not at all clear that both apply to the same system. Apart from the absence of electronic processes in both the theoretical and numerical models, an obvious uncertainty concerns the structure of amorphous Si, which is in all models assumed to be (statistically) homogeneous. However, it is known that a-Si contains structural inhomogeneities that lead, for instance, to the lower mass density of *a*-Si as compared to *c*-Si.[7] In 1970, Brodsky *et al.* already stated that bulk *a*-Si consists of building blocks with dimensions between 1 and 1.5 nm, and contains numerous internal microscopic surfaces.[26] More recently, electron microscopy studies have revealed that amorphous tetrahedral semiconductors like *a*-Si and *a*-Ge are structurally equivalent to a collection of polycrystalline grains with diameters less than 3 nm.[29] This concept is relevant from the point of view of our experiments. The presence of building blocks and microscopic surfaces may result in phonon confinement effects.

As a crude estimate for the length scale $\tilde{\lambda}$ that may be relevant for the properties of a certain acoustic mode, we divide the average sound velocity in *a*-Si (5×10^3 ms^{-1}) by the frequency of that mode. Hence, we find that $\tilde{\lambda} \gtrsim 1$ nm for frequencies $\lesssim 170$ cm^{-1}. Remarkably, we obtained mean decay times that were much longer for the modes with frequencies $\gtrsim 200$ cm^{-1} than for the modes with lower frequencies. We speculate that this may be a result of the high-frequency modes being ''trapped'' inside *a*-Si building blocks, rather than being localized in Anderson's sense. If the blocks are sufficiently decoupled from the surroundings, the anharmonic decay is suppressed when it involves the breakup of an eigenmode of the block into modes that have typical wavelengths not fitting the block dimensions. Also, the decay of modes with lower frequencies may be slower than in homogeneous structures. One form of decoupling one could

think of is the case that a large acoustic mismatch exists at the boundaries of the blocks, for instance, due to voids.

We emphasize that, in order to explain our results following this line of reasoning, it is not required that *all* building blocks are decoupled. As the experimental setup used is sensitive only to long-lived phonons, the behavior observed is not necessarily representative for all phonons. In this respect, it is of interest to perform new experiments with a setup sensitive to decay times much shorter than the lifetimes that Scholten *et al.* and we obtained. In addition, experimental[30] and theoretical studies on the dynamics of vibrations in mixed amorphous-nanocrystalline materials may provide further information on the possible relation between the observed anomalous vibrational properties and the microstructure of *a*-Si:H. More generally, detailed knowledge of the microstructure of amorphous Si may elucidate the remarkable findings.

V. CONCLUSIONS

In summary, we present results of pulsed Raman experiments on the population decay of optically excited phonons in hydrogenated Si. In all samples studied, mean decay times of ~ 70 ns were obtained for phonons with frequencies $\gtrsim 200\ \mathrm{cm}^{-1}$. The lower-energy modes appeared to have lifetimes shorter (<10 ns) than could be resolved with the experimental setup. The exact reason for the extremely long phonon lifetimes is still a matter of debate. It has been suggested that bulk *a*-Si consists of building blocks with dimensions between 1 and 1.5 nm, length scales that are likely to be relevant for the dynamics of vibrations of the frequencies studied. The idea that a portion of the phonons in *a*-Si:H have such long lifetimes because they are confined to nanometer scale regions in the amorphous structure is worth exploring further.

Apart from the relatively fast decays interpreted as phonon lifetimes, an additional slowly ($\gg 100$ ns) decaying contribution to the Raman signals was detected in *a*-Si:H films prepared by plasma enhanced chemical vapor deposition. This contribution was not observed in layers grown by hot-wire assisted chemical vapor deposition. A model is presented that qualitatively explains the slow background as resulting from electronic recombination processes. Further, it turns out that both relaxation of hot charge carriers and nonradiative recombination of free carriers with carriers localized in the tail states contribute significantly to the Raman signals. The ratio between the relaxation and recombination rates is demonstrated to depend on material parameters and the excitation power, and it determines if the slow contribution is observed or not. This proves that the pulsed Raman technique is sensitive to relative rates of electronic processes. Our results call for direct ultrafast optical measurements of these rates in HW material in order to find new clues to understanding the origin of the better stability of that material.

ACKNOWLEDGMENTS

The authors gratefully acknowledge F. J. M. Wollenberg, P. Jurrius, and C. R. de Kok for invaluable technical assistance, and C. H. M. van der Werf for growing the *a*-Si:H films. We thank G. D. J. Smit for assistance during the experiments and helpful discussions. This work is part of the research program of the Dutch foundation Stichting voor Fundamenteel Onderzoek der Materie (FOM), which is financially supported by the Nederlandse Organisatie voor Wetenschappelijk Onderzoek (NWO).

[1] A.J. Scholten, A.V. Akimov, and J.I. Dijkhuis, Phys. Rev. B **47**, 13 910 (1993); A.J. Scholten, P.A.W.E. Verleg, J.I. Dijkhuis, A.V. Akimov, R.S. Meltzer, and R. Orbach, Solid State Phenom. **44-46**, 289 (1995).

[2] J. Menendez and M. Cardona, Phys. Rev. B **29**, 2051 (1984).

[3] R. Orbach and A. Jagannathan, J. Phys. Chem. **98**, 7411 (1994); for a review, see T. Nakayama, K. Yakubo, and R.L. Orbach, Rev. Mod. Phys. **66**, 382 (1994).

[4] A.J. Scholten and J.I. Dijkhuis, Phys. Rev. B **53**, 3837 (1996).

[5] J. Fabian and P.B. Allen, Phys. Rev. Lett. **77**, 3839 (1996); P.B. Allen, J.L. Feldman, J. Fabian, and F. Wooten, Philos. Mag. B **79**, 1715 (1999).

[6] C. Tsang and R.A. Street, Phys. Rev. B **19**, 3027 (1979).

[7] R. Biswas, I. Kwon, A.M. Bouchard, C.M. Soukoulis, and G.S. Grest, Phys. Rev. B **39**, 5101 (1989).

[8] H. Meiling and R.E.I. Schropp, Appl. Phys. Lett. **70**, 2681 (1997); X. Liu, B.E. White, Jr., R.O. Pohl, E. Iwanizcko, K.M. Jones, A.H. Mahan, B.N. Nelson, R.S. Crandall, and S. Veprek, Phys. Rev. Lett. **78**, 4418 (1997).

[9] I.A. Shkrob and R.A. Crowell, Phys. Rev. B **57**, 12 207 (1998), and references therein.

[10] D.L. Staebler and C.R. Wronski, Appl. Phys. Lett. **31**, 292 (1977).

[11] H.M. Branz, Phys. Rev. B **59**, 5498 (1999); H.M. Branz, Solid State Commun. **105**, 387 (1998).

[12] A. Madan, P. Rava, R.E.I. Schropp, and B. von Roedern, Appl. Surf. Sci. **70/71**, 716 (1993).

[13] R.E.I. Schropp, K.F. Feenstra, E.C. Molenbroek, H. Meiling, and J.K. Rath, Philos. Mag. B **76**, 309 (1997).

[14] D. Beeman, R. Tsu, and M.F. Thorpe, Phys. Rev. B **32**, 874 (1985).

[15] K.F. Feenstra, R.E.I. Schropp, and W.F. van der Weg, J. Appl. Phys. **85**, 6843 (1999); K.F. Feenstra, Ph.D thesis, Utrecht University, 1998.

[16] Z. Vardeny and J. Tauc, Phys. Rev. Lett. **25**, 1223 (1981).

[17] J.E. Smith, M.H. Brodsky, B.L. Crowder, and M.I. Nathan, Phys. Rev. Lett. **26**, 642 (1971).

[18] Those *a*-Si:H layers were deposited by means of PE chemical vapor depositon, on sapphire substrates, at the A.F Ioffe Physical-Technical Institute in St. Petersburg.

[19] R. Stachowitz, M. Schubert, and W. Fuhs, J. Non-Cryst. Solids **227**, 190 (1998).

[20] R.I. Devlen, G.S. Kanner, Z. Vardeny, and J. Tauc, Solid State Commun. **78**, 665 (1991).

[21] P.M. Fauchet, D. Hulin, R. Vanderhaghen, A. Mourchid, and W.L. Nighan Jr., J. Non-Cryst. Solids **141**, 76 (1992); P.M. Fauchet, D. Hulin, A. Migus, A. Antonetti, J. Kolodzey, and S. Wagner, Phys. Rev. Lett. **57**, 2438 (1986).

[22] A. Esser, K. Seibert, H. Kurz, G.N. Parsons, C. Wang, B.N. Davidson, G. Lucovsky, and R.J. Nemanich, Phys. Rev. B **41**, 2879 (1990).
[23] A.A. Kaplyanskii, A.V. Akimov, S.A. Basun, S.P. Feofilov, E.S. Moskalenko, J. Kočka, and J. Stuchlik, J. Lumin. **53**, 7 (1992).
[24] A.J. Scholten, A.V. Akimov, and J.I. Dijkhuis, Phys. Rev. B **54**, 12 151 (1996).
[25] M. van der Voort, C.W. Rella, A.F.G. van der Meer, A.V. Akimov, and J.I. Dijkhuis, Phys. Rev. Lett. **84**, 1236 (2000).
[26] M.H. Brodsky, R.S. Title, K. Weiser, and G.D. Petit, Phys. Rev. B **1**, 2632 (1970).
[27] T. Damker, H. Böttger, and V.V. Bryksin, Phys. Rev. B **59**, 8626 (1999).
[28] S.R. Bickham, Phys. Rev. B **59**, 4894 (1999); S.R. Bickham and J.L. Feldman, *ibid.* **57**, 12 234 (1998).
[29] M.M.J. Treacy, J.M. Gibson, and P.J. Keblinski, J. Non-Cryst. Solids **231**, 99 (1998); M.M.J. Treacy, P.M. Voyles, and J.M. Gibson, J. Non-Cryst. Solids **266-269**, 150 (2000); J.M. Gibson and M.M.J. Treacy, Phys. Rev. Lett. **78**, 1074 (1997).
[30] M. van der Voort, O.L. Muskens, A.V. Akimov, A.B. Pevtson, and J.I. Dijkhuis (unpublished).